Structure and Magnetic Properties of Sputtered Nd-Fe-B Alloys

Ya.L. Linetsky and N.V. Kornilov

Studies were conducted on the relationship between the composition of Nd-Fe-B alloys, the temperature of the substrate, additional heat treatment and magnetic properties, crystalline phases, and microstructure and texture of films 30 to 300 μm thick produced by ion-plasma sputtering of cast targets. The sputtering rate was maintained at ~30 μm/h. The axial crystalline texture (001) along the normal to the sputtering plane is formed at a sputtering temperature within the limits ranging from 300 to 450 °C and higher than 600 °C. In the intermediate domain of sputtering temperatures, there is a deterioration of the texture (001), or such a change of the indices of the texture when the normal to one of the planes of the zone [010] becomes its axis. Within the framework of the classical theory of crystallization, a model of growth texture formation during the course of sputtering is suggested. The model explains the nonmonotonic change of texture with the change of sputtering temperature. The data obtained about the structure and properties of films have made it possible to optimize the sputtering process with a view to obtaining sputtered magnets with very good permanent magnet properties. Examples of magnetic systems and devices with sputtered magnets are given.

Keywords

magnetic properties, magnetic films,
rare earth alloys, sputtered permanent magnets

1. Introduction

PROGRESS in modern technology indicates a trend toward the use of integrated magnetic circuits in electrical machinery and instrumentation. Magnetic systems, including multilayer ones, can be obtained by sputtering magnetically hard materials on a magnetically soft or nonmagnetic substrate. Current methods of physical vacuum sputtering make it possible to obtain magnetically hard films 10^{-1} to 10^{2} μm thick. Systems with complex topography of magnetic field can be created through the sputtering of structures from layers with different magnetic hardness. Films and coatings can be magnetically isotropic, possess well-defined lines in the sputtering plane, or be characterized by perpendicular anisotropy. Sputtering on a substrate at room temperature of alloys Sm-Co (Ref 1-3) and Nd-Fe-B (Ref 3, 4) yields isotropic magnetic films, which assume large magnetic hardness in the course of heat treatment. Sputtering onto the hot substrate gives Sm-Co films in which the easy magnetization axis lies in the sputtering plane (Ref 5) and Nd-Fe-B films with the easy magnetization axis perpendicular to the sputtering plane (Ref 3, 6, 7, 8). In Ref 5 and 6, methods of obtaining films of 1 to 2 μm thickness and their magnetic properties are described, while in Ref 3, 7,and, 8 data for films 30 to 200 μm thick are given.

The sputtering temperature (T_s) and sputtering rate (V_s) are the main parameters of the sputtering process determining structure and magnetic properties of films. Magnetic fields exceeding 10 mT are needed for miniature electric motors, magnetic field sensors, and accelerometers. Such fields can be obtained from sputtered magnets 30 to 300 μm thick. For example a magnet of the Nd-Fe-B alloy with the dimensions in the sputtering plane 1.5 by 1.5 mm and 0.2 mm thick produced a magnetic field of about 60 mT on the surface. A sputtering rate not less than 20 μm/h was needed to obtain magnets of such thickness.

The objective of this paper is to show how the composition, sputtering temperature, and heat treatment influence structure and magnetic properties of thick films of (Nd,Dy,Tb)-(Fe,Co)-B alloys.

2. Experimental Techniques

The 100-μm-thick films were obtained by sputtering with the use of a three-electrode scheme of the cast target. Magnetic focusing of an Ar-plasma was used. The sputtering rate was about 30 μm/h. The temperature of the substrate (Cu or Ta) was maintained by a resistance heater within prescribed limits. The temperature of the substrate T_s was measured by a thermocouple from the side opposite to the plasma. Magnetic properties of films detached from the substrate were measured with a vibrating sample magnetometer with a maximum field of 2500 kA/m. Some films were initially magnetized with a pulse field of 8000 kA/m. The density of sputtered alloys in calculations was assumed equal to 7.6×10^3 kg/m^3.

The films were separated from the substrate mechanically. Prior to the magnetic measurements, the films were subjected to electrolytic etching to remove the transition layer formed between the film and the substrate in the course of sputtering. Chemical composition of the target and films was determined by the atomic emission spectral method. Two groups of alloys differing from each other by the content of rare earth metal (REM) and boron were sputtered.

Compositions of sputtered alloys differed little from compositions of the corresponding targets summarized in Table 1. However, the films contained additionally 0.2 to 0.9 mass percent Cu due to the sputtering of the holders of the target. Struc-

Ya.L. Linetsky and **N.V. Kornilov**, Laboratory for the Technology of Magnetic Film Systems, Moscow Institute of Steel and Alloys, 4 Leninsky Prospekt, Moscow, 117936, Russia. E-mail: yavlin @ engin.umich.edu

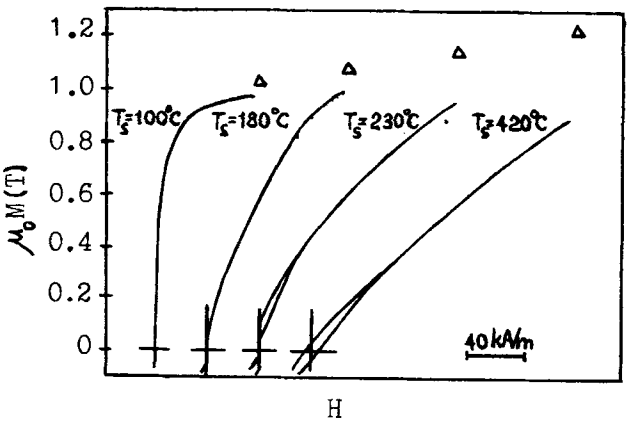

Fig. 1 Magnetic hysteresis curves (with due account of the demagnetizing factor) measured in the plane of the films of alloy 1 sputtered at T_s of 420 °C or less. Δ are $M^{\parallel}$ values for each film in the field 2.5 MA/m.

Table 1 Chemical composition of targets for sputtering

No.	Alloy composition
1	$Nd_{16}Fe_{76}B_8$
2	$(Nd_{0.843}Tb_{0.094}Dy_{0.063})_{16}(Fe_{0.934}Co_{0.066})_{76}B_8$
3	$(Nd_{0.843}Tb_{0.094}Dy_{0.063})_{16}(Fe_{0.85}Co_{0.15})_{76}B_8$
4	$Nd_{17.5}Fe_{73.5}B_9$
5	$(Nd_{0.843}Tb_{0.094}Dy_{0.063})_{17.5}(Fe_{0.934}Co_{0.066})_{73.5}B_9$
6	$(Nd_{0.843}Tb_{0.094}Dy_{0.063})_{17.5}(Fe_{0.85}Co_{0.15})_{73.5}B_9$

tural studies were conducted employing an x-ray diffractometer with Fe-K_α radiation.

3. Results

3.1 *Perpendicular Magnetic Anisotropy*

Films of all alloys sputtered at T_s of 450 °C or less have coercive force, ${}_iH_c$ equal to 1 to 10 kA/m. Lowering the T_s results in a decrease of ${}_iH_c$. Magnetization curves of such films in the direction perpendicular to the sputtering plane practically coincide with the coordinate axis of magnetization. Hysteresis loops of the first alloy (Table 1) in the sputtering plane for T_s from 100 to 420 °C are shown in Fig. 1. It is evident that the higher the T_s within the temperature range under consideration, the greater the inclination of the hysteresis loop measured in the sputtering plane to the coordinate axis of magnetization and the stronger the hysteresis itself. Differences in variation of magnetization curves and in the shape of hysteresis loops in the sputtering plane and along the normal to it testify to the fact that at T_s greater than 100 °C a macroscopic perpendicular anisotropy is developed in the film. X-ray structural analysis (gives an amorphous halo) and thermomagnetic analysis (Curie temperature of 448 K) indicates that the films sputtered at temperatures lower than 450 °C possess an amorphous structure.

Perpendicular anisotropy and magnetic hysteresis of amorphous films can be considerably enhanced with the aid of heat treatment. During heat treatment, the amorphous structure of

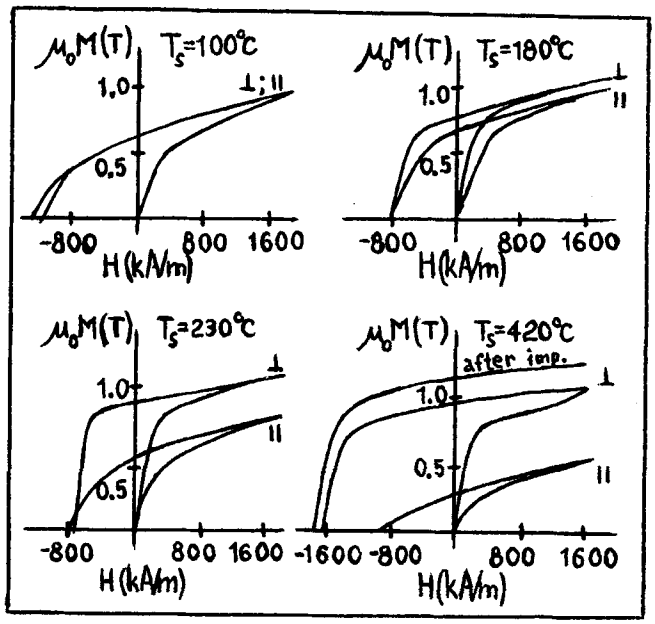

Fig. 2 Magnetic hysteresis curves (with due account of the demagnetizing factor) measured perpendicular (⊥) and parallel (||) to the film plane of alloy 1. The films are sputtered at T_s of 420 °C or less and annealed at 700 °C for 30 min.

films transforms into a crystalline structure. Films isotropic in the amorphous state also retain their magnetic isotropy after heat treatment. Anisotropy of the magnetic hysteresis of amorphous films after heat treatment and crystallization is enhanced with the increase of T_s from 180 to 420 °C (see Fig. 2).

Thus, local axes of easy magnetization of clusters in the inhomogeneous amorphous structure, which form in the course of sputtering at T_s greater than 100 °C and less than 450 °C, are predominantly oriented along the normal to the film surface. Within the limits of the above-mentioned temperature range, larger values of T_s result in a better magnetic orientation.

Apparently, clusters play the role of three-dimensional embryos of the process of crystallization in the course of sputtering. Then the texture corresponding to the predominant spatial orientation of clusters, as well as the texture of [001] of such films after crystallization, can be regarded as textures of nucleation.

Sputtering at temperatures higher than 450 °C gives a crystalline structure where the $Nd_2Fe_{14}B$ (2:14:1) phase is the main component. Figure 3 illustrates dependencies of the remanence $M_r^{\perp}$ measured in a direction perpendicular to the film as a function of the sputtering temperature, T_s. Values of $M_r^{\perp}$ for T_s in the 400 to 450 °C range are given after the heat treatment of films at 700 °C for 30 min. Other data are obtained directly after sputtering. It is evident from Fig. 3 that for all alloys in the T_s range of 500 to 600 °C, there is a minimum of remanence, $M_r^{\perp}$, while for alloys 1 and 4, $M_r^{\perp}$ versus T_s curves have two minima in this temperature range. The higher the cobalt content in the film, the lower the height of the $M_r^{\perp}$maximum in the low temperature range and the deeper the minimum in the interval of 500 to 600 °C.

Table 2 Phase composition of alloys sputtered at different temperatures

Alloy composition	Phases in films	
	$T_s \leq 450$ °C + annealing 700 °C, 30 min	500 °C $\leq T_s \leq$ 700 °C
$Nd_{16}Fe_{76}B_8$	(1) $Nd_2Fe_{14}B$ (a = 0.880 nm, c = 1.219 nm) (2) Nd_2O_3 ($P321$) (3) $Nd_{1.1}Fe_4B_4$ (4) αNd ($P63/mmc$) (5) bcc phase (a = 1.02 nm)	Same as for $T_s \leq 450$ °C after annealing
$(Nd_{0.843}Tb_{0.094}Dy_{0.063})_{16}(Fe_{0.934}Co_{0.066})_{76}B_8$ or $(Nd_{0.843}Tb_{0.094}Dy_{0.063})_{17.5}(Fe_{0.934}Co_{0.066})_{73.5}B_9$	(1) $(Nd,Tb,Dy)_2(Fe,Co)_{14}B$ (a = 0.877 nm, c = 1.216 nm) (2) R_2O^3 (3) $(Nd,Tb,Dy)_{1.1}Fe_4B_4$ (4) αNd (5) βNd ($1m\bar{3}m$, a = 0.413 nm) (6) bcc phase (a = 1.02 nm)	Same as for $T_s \leq 450$ °C after annealing + R(Fe,Co)2 ($Fd3m$, a = 0.74 nm)
$(Nd_{0.843}Tb_{0.094}Dy_{0.063})_{16}(Fe_{0.85}Co_{0.15})_{76}B_8$ or $(Nd_{0.843}Tb_{0.094}Dy_{0.063})_{17.5}(Fe_{0.85}Co_{0.15})_{73.5}B_9$	(1) $(Nd,Tb,Dy)_2(Fe,Co)_{14}B$ (a = 0.876 nm, c = 1.214 nm) (2) R_2O^3 (3) $(Nd,Tb,Dy)_{1.1}Fe_4B_4$ (4) αNd, βNd (5) bcc phase (a = 1.02 nm)	Same as for $T_s \leq 450$ °C after annealing + R(Fe,Co)2 (a = 0.74 nm)

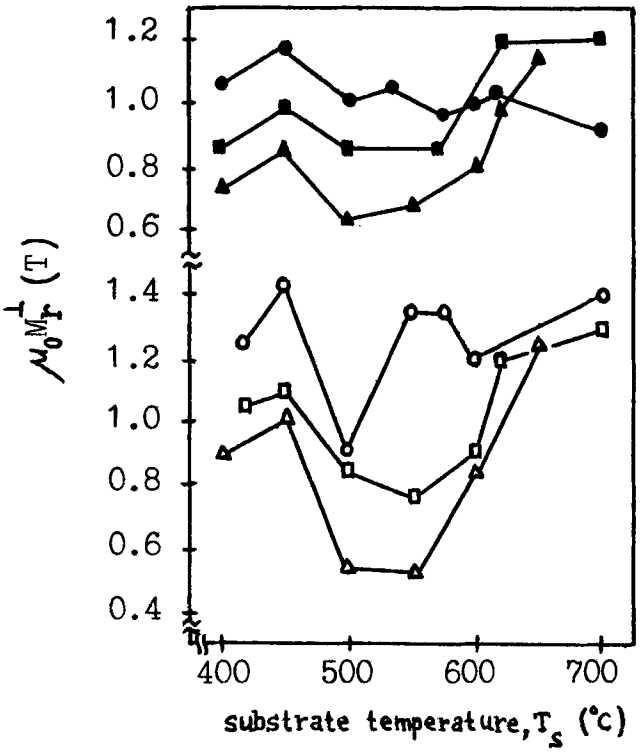

Fig. 3 The impact of the substrate temperature on the residual induction $M_r^{\perp}$ perpendicular to the film. For T_s equal to 400, 420, and 450 °C, the data are given after annealing at 700 °C for 30 min and magnetization in the pulse field. ○ $Nd_{16}Fe_{76}B_8$. ● $Nd_{17.5}Fe_{73.5}B_9$. □ $(Nd,Tb,Dy)_{16}(Fe_{0.934}Co_{0.066})_{76}B_8$. ■ $(Nd,Tb,Dy)_{17.5}(Fe_{0.934}Co_{0.066})_{73.5}B_9$. Δ $(Nd,Tb,Dy)_{16}(Fe_{0.85}Co_{0.15})_{76}B_8$. ▲ $(Nd,Tb,Dy)_{17.5}(Fe_{0.85}Co_{0.15})_{73.5}B_9$.

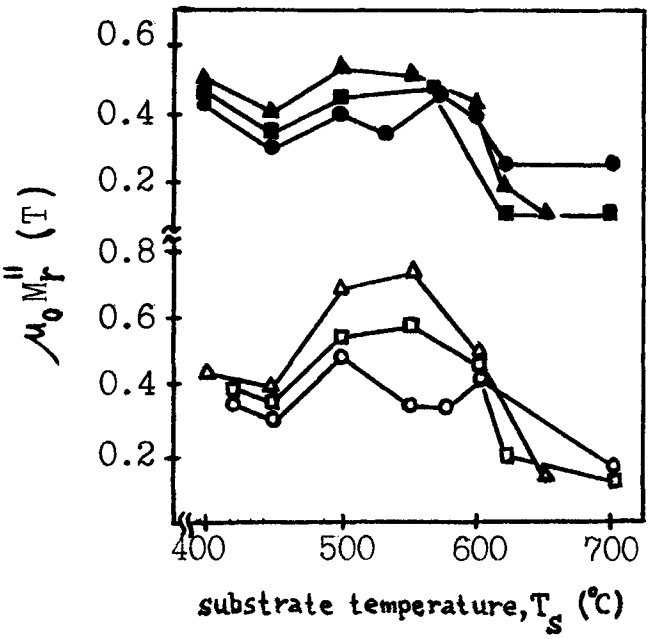

Fig. 4 Influence of the substrate temperature on residual induction $M_r^{\perp\parallel}$ parallel to the film. For T_s equal to 400, 420, and 450 °C, the data are provided after annealing at 700 °C for 30 min. Designations of the curves are the same as in Fig. 3.

$M_r^{\parallel}$ versus T_s curves for residual induction measured in the sputtering plane are given in Fig. 4. Comparison of Fig. 3 and 4 shows that $M_r^{\parallel}$ (T_s) curves are practically mirror reflection $M_r^{\parallel}$ (T_s) curves. Changes in the crystalline texture may be a reason for the systematic variation of $M_r^{\parallel}$ (Ts) and $M_r^{\perp}$ (Ts) curves.

3.2 *Crystalline Texture*

Reverse pole figures were constructed to determine the crystalline texture in films. Pole densities, P_{hkl}, were calculated employing:

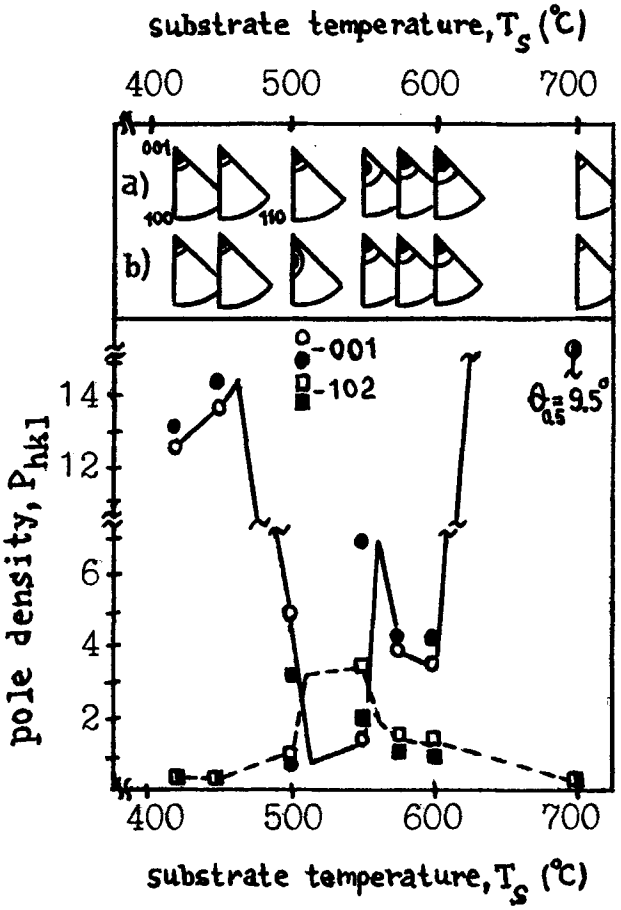

Fig. 5 Influence of the sputtering temperature on the crystalline texture in films of the $Nd_{16}Fe_{76}B_8$ alloy. For T_s equal to 420 and 450 °C, data are given after annealing at 700 °C for 30 min. For the upper part: (a) is pole figures for the side near the substrate and (b) is pole figures for free surface of the film. For the lower part: pole densities P_{hkl} for *hkl* are ○,● 006 and □,■ 204; ○ and □ are the side of the substrate; and ● and ■ are the free side.

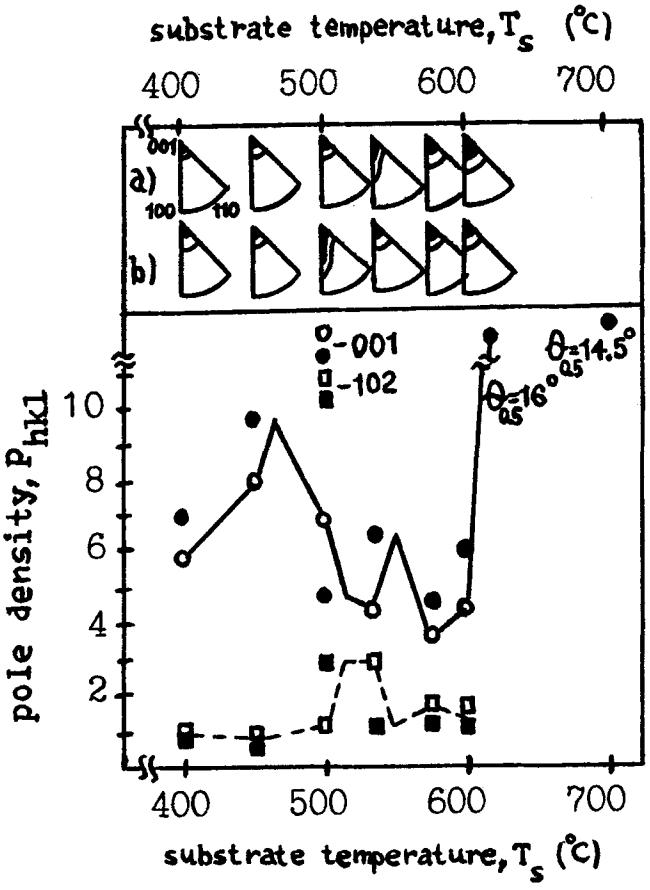

Fig. 6 Influence of the sputtering temperature on the crystalline texture in films of the $Nd_{17.5}Fe_{73.5}B_9$ alloy. For T_s equal to 400 and 450 °C, data are given after annealing at 700 °C for 30 min. For the upper part: (a) is pole figures for the side near the substrate and (b) is pole figures for free surface of the film. For the lower part: pole densities P_{hkl} for *hkl* are ○,● 006 and □,■ 202; ○ and □ are the side of the substrate; and ● and ■ are the free side.

$$P_{hkl} = \frac{(I^n_{HKL}/I^0_{HKL}) \sum_n M_{hkl}}{\sum_n (M_{hlk} I^n_{HKL}/I_{HKL})^0} \qquad \text{(Eq 1)}$$

where I^n_{HKL} and I^0_{HKL} are the measured and calculated intensities of the *HKL* line on the x-ray photograph for the sample and the reference, respectively, and M_{hkl} is the multiplicity factor for the *hkl* plane.

Two rows of pole figures are given in the upper part of Fig. 5 to 10. The upper row is plotted from the results of the x-ray photography of films from the substrate side whereas the lower row is from the free side. The apexes of pole figures indicate the sputtering temperature. In the lower part of Fig. 5 to 10, P_{hkl} (T_s) dependencies for the plane (001) and a few other planes are given in the direction of normals to which the texture axis is displaced when T_s changes. Curves for P_{hkl} are plotted from experimental data for the free and reverse sides of films with due account of the temperature variation across the thickness of the films. This temperature differential for Nd-Fe-B films 100 μm thick makes up about 15 °C. This differential is estimated from the results of the experiment with the use of substrates, which differ greatly in heat conduction (Cu and mica), and this temperature change originates due to the fact that the heating of the substrate takes place mainly due to the plasma radiation.

It is seen that all films are characterized by axial crystalline texture. For films of all alloys sputtered at 400 to 450 °C and higher than 600 °C, the texture axis is [001]. Films sputtered at T_s greater than 600 °C have a sharp texture. The width at half of the height of the oscillation curve $\Theta_{0.5}$ of 066 reflection has been used as its characteristic.

In the range of sputtering temperatures from 500 to 600 °C, the axial texture [001] is considerably attenuated in case of its slight local enhancement at T_s equal to 550 to 575 °C. In this domain of T_s, the following textures are observed for alloys for different composition: the blurred axial texture [001] with the

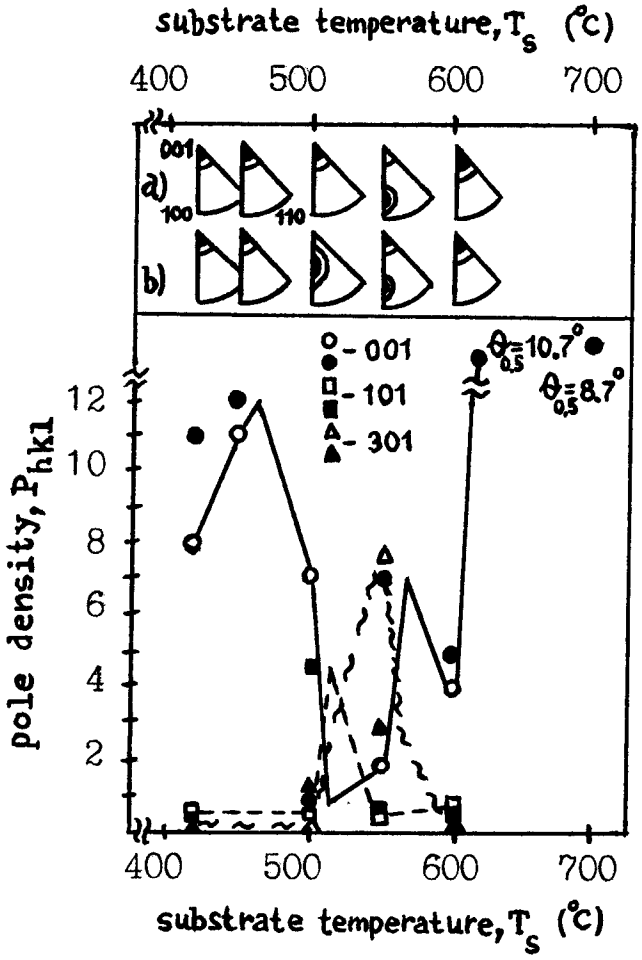

Fig. 7 Influence of the sputtering temperature on the crystalline texture in films of the $(Nd,Tb,Dy)_{16}(Fe_{0.934}Co_{0.066})_{76}B_8$ alloy. For T_s equal to 420 and 450 °C, data are given after annealing at 700 °C for 30 min. For the upper part: (a) is pole figures for the side near the substrate and (b) is pole figures for free surface of the film. For the lower part: pole densities P_{hkl} for *hkl* are ○,● 006, □,■ 202, and Δ,▲ 301; ○, □, and D are the side of the substrate; and ●, ■, and ▲ are the free side.

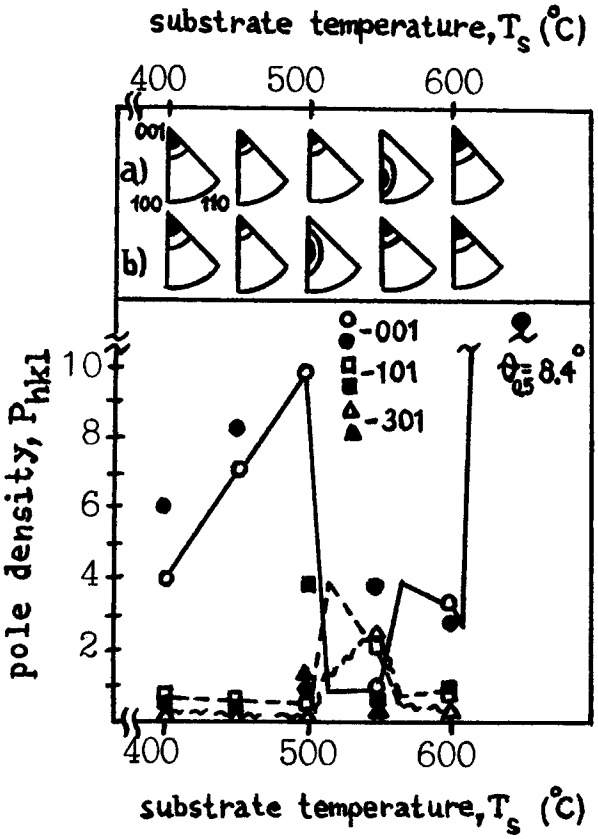

Fig. 8 Influence of the sputtering temperature on the crystalline texture in films of the $(Nd,Tb,Dy)_{16}(Fe_{0.85}Co_{0.15})_{76}B_8$ alloy. For T_s equal to 400 and 450 °C, data are given after annealing at 700 °C for 30 min. For the upper part: (a) is pole figures for the side near the substrate and (b) is pole figures for free surface of the film. For the lower part: pole densities P_{hkl} for *hkl* are ○,● 006, □,■ 202, and Δ,▲ 301; ○, □, and Δ are the side of the substrate; and ●, ■, and ▲ are the free side.

slight increase of pole densities for planes of the zone [010] with respect to the ideal axial texture; distorted axial texture [001] characterized by the increase of P_{hkl} as planes are approaching the [010] zone; axial texture [uOw] with the axis which is normal to the plane belonging to the zone [010]; and two-component texture with axes [001] and the normal to the plane (201) or (301).

Experimentally observed dependencies of the texture can be explained by the hypothesis that in addition to the fixed texture of nucleation [001], during the sputtering of crystalline films, the development of the axial growth texture [100] or [001] takes place.

The resulting texture observed in films sputtered at 500 to 600 °C is formed under the influence of two textures: the nucleation texture [001] and the growth [100] texture. Representing the distribution function of probabilities of the orientation of grains for the aggregate event—the nucleation and the growth—as a product of distribution functions of orientations for nucleation and growth, it is possible to obtain a variety of textures observed in this interval of the sputtering temperatures. All obtained texture varieties have poles belonging to the zone [010] since each of the planes of this zone makes up the least total angle with the planes (001) and (100) and, therefore, must have the greatest overlapping of the probability distribution functions for both textures (nucleation and growth) with axes [001] and [100].

In the course of sputtering at temperatures higher than 600 °C, a growth texture [001] develops. Overlapping the same orientation texture results in the development of a strong [001] texture.

Comparison of Fig. 5, 7, and 8 and 6, 9, and 10 shows that the increase in the content of rare-earth metals and boron in the alloy leads to a certain weakening of the texture [001] of films obtained by annealing from the anisotropic amorphous state. It also causes the enhancement of the texture [001] and the weakening of the texture of $[\bar{u}O\bar{w}]$ in the T_s interval from 500 to 600

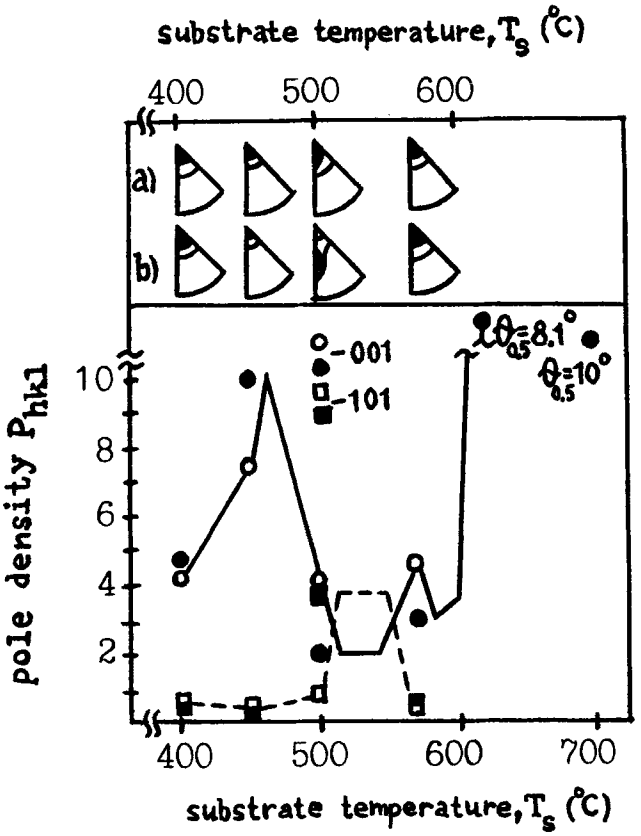

Fig. 9 Influence of the sputtering temperature on the crystalline texture in films of the $(Nd,Tb,Dy)_{17.5}(Fe_{0.934}Co_{0.066})_{73.5}B_9$ alloy. For T_s equal to 400 and 450 °C, data are given after annealing at 700 °C for 30 min. For the upper part: (a) is pole figures for the side near the substrate and (b) is pole figures for free surface of the film. For the lower part: pole densities P_{hkl} for *hkl* are ○,● 006 and □,■ 202; ○ and □ are the side of the substrate; and ● and ■ are the free side.

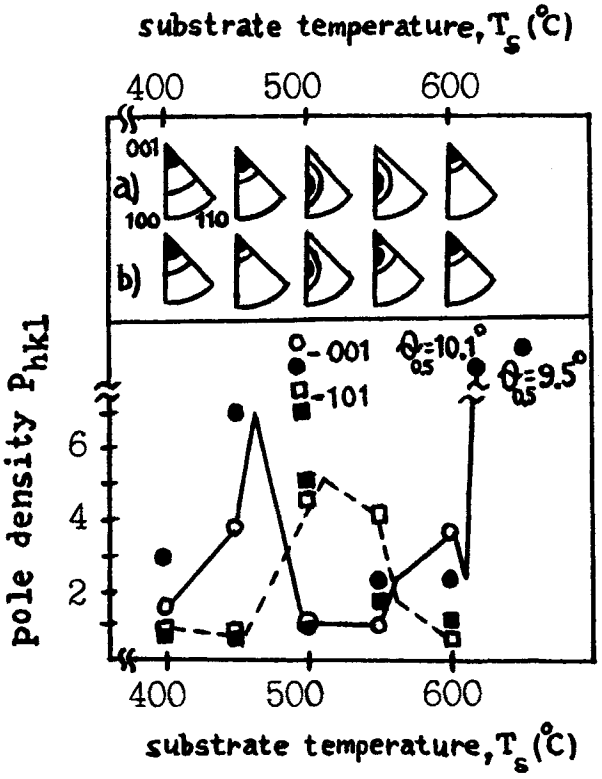

Fig. 10 Influence of the sputtering temperature on the crystalline texture in films of the $(Nd,Tb,Dy)_{17.5}(Fe_{0.85}Co_{0.15})_{73.5}B_9$ alloy. For T_s equal to 400 and 450 °C, data are given after annealing at 700 °C for 30 min. For the upper part: (a) is pole figures for the side near the substrate and (b) is pole figures for free surface of the film. For the lower part: pole densities P_{hkl} for *hkl* are ○,● 006 and □,■ 202; ○ and □ are the side of the substrate; and ● and ■ are the free side.

°C. In other words, the increase in the content of rare-earth metals and boron in the alloy somewhat weakens the texture of nucleation, but increases its weight in shaping the total texture in the domain of the texture of growth [100]. This is easily explained by the hypothesis that new grains of the $Nd_{23}Fe_{14}B$ phase come into being predominantly in the process of sputtering on admixture phases the amount of which rises with clearing away the composition of the alloy from stoichiometric $Nd_2Fe_{14}B$.

3.3 *Coercive Force and Structure*

The impact of sputtering temperature on the coercive force in the direction perpendicular to the film, ${}_iH_c^{\perp}$, is shown in Fig. 11 and 12. The dependence of ${}_iH_c^{\perp}$ versus T_c for all alloys has the same type of behavior. Comparison of curves in Fig. 11 and 12 shows that the increase in the content of Nd from 16 to 17.5 at.% and B from 8 to 9 at.% increases the maximum of ${}_iH_c^{\perp}$ and also increases the width of the sputtering temperature range where ${}_iH_c^{\perp}$ reaches its maximum value. Further, introduction of Tb and Dy into the sputtered alloy enhances the maximum of ${}_iH_c^{\perp}$ while the increase of cobalt content from 0.066 to 0.15 at.% in(Fe_xCo_{1-x}) does not change ${}_iH_c^{\perp}$.

The variation of ${}_iH_c^{\perp}$ (T_s) curves reflects the influence of atomic structure and morphology on the remagnetization of alloys. The phase composition of alloys is given in Table 2.

Sputtering at a temperature lower than 450 °C gives an amorphous structure, whereas at T_s greater than 500 °C, a crystalline structure is formed. In crystalline Nd-Fe-B alloys, phases 2:14:1, $NdFe_4B_4$, αNd, Nd_2O_3, and a phase with the bcc structure are detected. The phase composition of sputtered (Nd,Tb,Dy)-(Fe,Co)-B films depends on their prehistory. In the structure of these alloys in the amorphous state, the same phases are detected after annealing as in the crystalline ternary alloys. In addition to this, they also contain a cubic modification of Nd. After sputtering, the crystalline five-component alloys contain, in addition to the above-mentioned phases obtained through annealing of the amorphous structure, the $R(Fe,Co)_2$ Laves phase with an fcc structure.

In the sputtering process of alloys of all compositions at T_s higher than 620 °C, a eutectic composition is in the liquid state and is squeezed out onto the surface of the growing film. Thus,

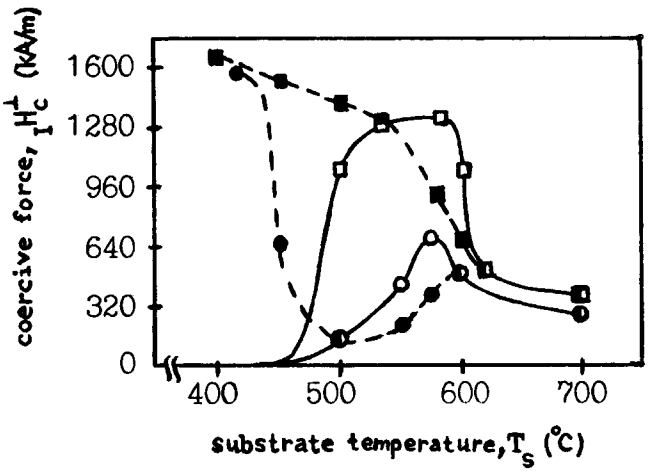

Fig. 11 Influence of substrate temperature, T_S, on the coercive force, $_iH_c^\perp$. O, □: after sputtering. ●, ■: after annealing at 700 °C for 30 min. O, ●: $Nd_{16}Fe_{76}B_8$. □, ■: $Nd_{17.5}Fe_{73.5}B_9$.

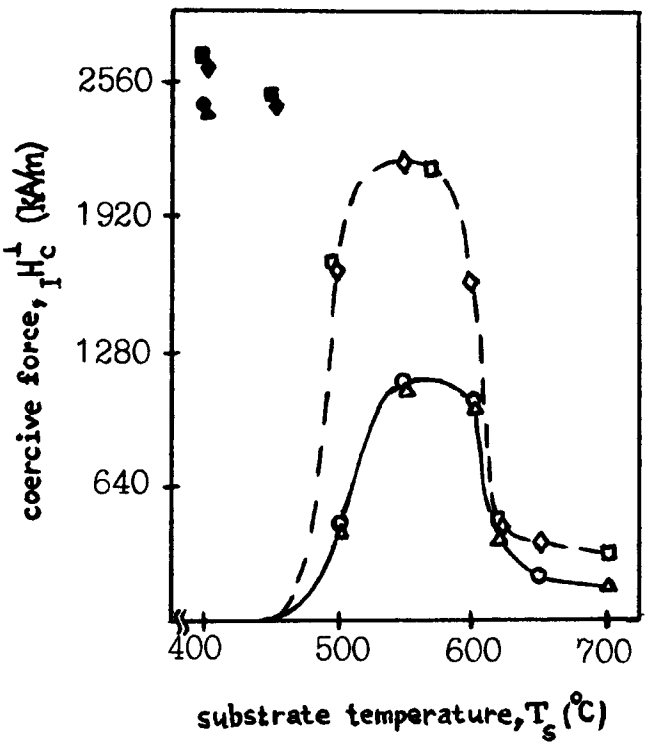

Fig. 12 Influence of the substrate temperature, T_S, on the coercive force, $_iH_c^\perp$. O, ●: $(Nd,Tb,Dy)_{16}(Fe_{0.934}Co_{0.066})_{76}B_8$. Δ, ▲: $(Nd,Tb,Dy)_{16}(Fe_{0.85}Co_{0.15})_{76}B$ ◊, ♦: $(Nd,Tb,Dy)_{17.5}(Fe_{0.934}Co_{0.066})_{76}B_9$. □, ■: $(Nd,Tb,Dy)_{17.5}(Fe_{0.85}Co_{0.15})_{73.5}B_9$. ●, ■, ♦, ▲: after annealing at 700 °C for 30 min. O, □, ◊, Δ: after sputtering.

the film surface gets accumulated with the eutectic in the form of drops. On x-ray photographs of such films, reflections from αNd for alloys 1 and 4 or reflections from αNd and βNd for other alloys are sharply intensified. Reflections from neodymium are weakened after mechanical removal of the frozen drops of the eutectic component and etching of the surface layer.

An electron microscope study was carried out on films of the $Nd_{16}Fe_{76}B_8$ alloy. After sputtering at 575 °C, the grain size of the phase 2:14:1 was within the limits of 0.3 to 0.6 μm. Some round extended inclusions of impurity phases with dimensions of 0.04 to 0.1 μm were observed inside the grains at the triple junctions. After sputtering at 700 °C, the size of the phase 2:14:1 grains reached several micrometers. Thus, the ascending branch of the $_iH_c^\perp$ versus T_s curve is influenced by the transition of the amorphous maximum structure into the crystalline structure. At the $_iH_c^\perp$ maximum, the structure consists of a fine-grained 2:14:1 and of impurity nonmagnetic phases, whereas the descending branch of the $_iH_c^\perp(T_s)$ curve corresponds to the fast growth of grains and to the change in the film composition due to squeezing out the liquid eutectics onto the surface.

As noted above, heat treatment exerts considerable influence on the structure and magnetic properties of films. Annealing at temperatures ranging from 650 to 700 °C resulted in a sharp increase of $_iH_c^\perp$ for all alloys sputtered at T_s less than 450 °C (see curves 2 in Fig. 11 and individual points in Fig. 12). The maximum permissible level of $_iH_c^\perp$ after the thermal treatment of alloys with the initial amorphous structure rises in the case of replacement of Nd by heavy REM, but does not vary in the case of simultaneous decrease of Nd content from 17.5 to 16 at.% and B content from 9 to 8 at.%. This constitutes the difference between the behavior of $_iH_c^\perp$ of films sputtered in the amorphous state from the behavior of $_iH_c^\perp$ of films fallen out with the crystalline structure whose height of the maximum on $_iH_c^\perp(T_s)$ curves decreased almost by 50% with the same decrease of Nd and B content. However, further decrease of REM and B content also causes a decrease of $_iH_c^\perp$ in alloys sputtered in the amorphous condition and treated by heat. For example in the authors' experiments, the decrease of Nd concentration from 16 to 13 at.% and B concentration from 8 to 6 at.% was accompanied by the decrease of $_iH_c^\perp$ from 1600 to 480 kA/m.

The large coercive force, $_iH_c^\perp$, after annealing amorphous films is accounted for by the high degree of dispersity and by the homogeneity of the microstructure. Grains of the phase 2:14:1 have a regular shape. Their diameter lies within the limits ranging from 0.1 to 0.5 μm.

4. Applications

Films with a high degree of crystalline texture [001] are characterized by the rectangular magnetic hysteresis loop. The technology developed allows one to produce sputtered permanent magnets with a wide variety of magnetic characteristics: from $_iH_c^\perp = 2600$ kA/m, $\mu_0 M_r^\perp = 1.0T$, $(BH)_{max} = 195$ kJ/m^3 to $_iH_c^\perp = 640$ kA/m, $\mu_0 M_r^\perp = 1.35T$, $(BH)_{max} = 352$ kJ/m^3. Demagnetization curves of films with magnetic properties in the above range are given in Fig. 13.

Subsequent sputtering of alloys with different combinations of $M^\perp$ and $_iH_c^\perp$ allows one to obtain magnetic systems with sign-alternating poles of complex configurations.

The sputtering technology described in this paper was applied in manufacturing of a number of magnetic systems of different sensors and rotors of very small electric motors.

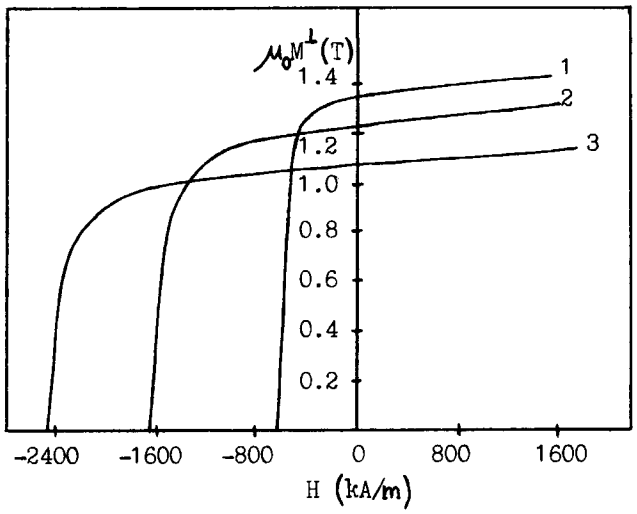

Fig. 13 Magnetization reversal curves (with due account of the demagnetizing factor) of films of the (Nd,Tb,Dy)-(Fe-Co)-B alloy. 1: alloy #1 sputtered at 575 °C. 2: alloy #1 sputtered at 420 °C and annealed at 700 °C for 30 min. 3: alloy #2 sputtered at 420 °C and annealed at 700 °C for 30 min.

5. Conclusions

Dependencies $M_r^{\perp}(T_s)$ and ${}_iH_c^{\perp}(T_s)$ given above show that in the course of sputtering of (Nd,Tb,Dy)-(Fe,Co)-B alloys at a rate of 30 μm/h, there are narrow intervals of values of the sputtering temperature in which films with high characteristics of magnetic hysteresis can be obtained. The emergence of the wide dip on the $M_r^{\perp}$ (T_s) curve is caused either by the deterioration of the crystalline texture [001], or by change of the indices of the texture axis. This change of indices occurs in such a direction that the normal to one of the planes of the zone [010] becomes the texture axis.

As demonstrated experimentally, in the course of sputtering at low temperatures in inhomogeneous amorphous films, a texture similar to the (001) texture forms.

Crystalline films with the axial texture [001], which possesses high $M_r^{\perp}$ and ${}_iH_c^{\perp}$, can be obtained by heat treatment from films with the inhomogeneous amorphous anisotropic structure.

Acknowledgments

Dr. Yan L. Linetsky is grateful to Dr. S.G. Sankar of Carnegie Mellon University, Dr. J.A. Salsgiver of Allegheny Ludlum Steel, and Dr. C.J. Painter of Westinghouse Science and Technology Center for their invitation to Materials Week. He is also pleased to thank Dr. S.G. Sankar for his kind hospitality in Pittsburgh. The results of this investigation were presented at Materials Week '93 in Pittsburgh by Dr. Ya.L. Linetsky.

References

1. V.V. Kotunov, B.P. Nam, and B.G. Lifshits, *Izv. V.U.Z. Chernaya Metall.*, (No. 3), 1982, p 91 (in Russian)
2. Y.L. Linetsky and I.P. Salo, *Izv. Akad. Nauk SSSR, Met.*, (No. 6), 1988, p 141 (in Russian)
3. B.S. Vekshin, B.A. Kapitanov, N.V. Kornilov, Y.L. Linetsky, V.M. Raigorodsky, and V.Y. Tsvetkov, *Elektrotechnika*, (No. 11), 1989, p 18 (in Russian)
4. V.M. Raigorodsky, Y.L. Linetsky, S.E. Sokolovsky, and V.Y. Tsvetkov, *Isv. V.U.Z. Chernaya Metall.*, (No. 9), 1990, p 56 (in Russian)
5. S.H. Aly, T.D. Cheung, L. Wickramasekara, and F.J. Cadieu, *J. Appl. Phys.*, Vol 57, (No. 6), 1985, p 2147
6. F.J. Cadieu, T.D. Cheung, and L. Wickramasekara, *J. Magn. Magn. Mater.*, Vol 54-57, 1986, p 535
7. V.A. Kapitanov, N.V. Kornilov, Y.L. Linetsky, and V.Yu Tsvetkov, *J. Magn. Magn. Mater.*, Vol 127, 1993, p 289-297
8. Y.L. Linetsky, V.M. Raigorodsky, and V.Y. Tsvetkov, *J. Alloy Comp., Vol 184, 1992, p 35*